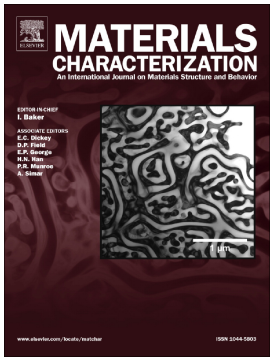

Nanostructural investigation of slightly altered rhyolitic volcanic glass

Viktoria Kovács Kis, Zsolt Czigány, Tibor Németh

PII: S1044-5803(16)31021-X
DOI: doi: 10.1016/j.matchar.2017.02.019
Reference: MTL 8571

To appear in: *Materials Characterization*

Received date: 21 November 2016
Revised date: 15 February 2017
Accepted date: 18 February 2017

Please cite this article as: Viktoria Kovács Kis, Zsolt Czigány, Tibor Németh , Nanostructural investigation of slightly altered rhyolitic volcanic glass. The address for the corresponding author was captured as affiliation for all authors. Please check if appropriate. Mtl(2017), doi: 10.1016/j.matchar.2017.02.019

Title: Nanostructural investigation of slightly altered rhyolitic volcanic glass

Authors: Viktoria Kovács Kis[a], Zsolt Czigány[a], Tibor Németh[b,c]

[a]Institute for Technical Physics and Materials Science, Centre for Energy Research, Hungarian Academy of Sciences H-1525 Budapest, POBox 49, Hungary

[b]Institute for Geological and Geochemical Research, Research Centre for Astronomy and Earth Sciences, Hungarian Academy of Sciences, H-1112 Budapest, 45 Budaörsi street, Hungary

[c]Department of Mineralogy, Eötvös Loránd University, H-1119 Budapest, Pázmány Péter sétány 1/c, Hungary

kis.viktoria@energia.mta.hu

czigany.zsolt@energia.mta.hu

ntibi@geochem.hu

Corresponding author: Viktoria Kovács Kis (kis.viktoria@energia.mta.hu)

Institute for Technical Physics and Materials Science, Centre for Energy Research, Hungarian Academy of Sciences H-1525 Budapest, POBox 49, Hungary

Abstract

Silica rich volcanic glass is investigated by selected area electron diffraction (SAED) and high resolution electron microscopy (HRTEM), and nanostructural characterisation is presented. In freshly crushed glass shards the presence of amorphous and randomly oriented nanocrystalline component was detected, the latter one enriched in iron with respect to the amorphous regions. To interpret the iron containing nanocrystalline structure, model clusters of different size, shape and composition were constructed and used to calculate scattered electron intensity. According to our calculations, already a single ring of six interconnected SiO_4 tetrahedra results a separate broad peak at ~5 Å which reflects nicely the main diffraction feature of amorphous silica. Inserting two dimensional iron array between two neighbouring silica layers produces a less compact structure and the first diffraction peak shifts towards larger values with respect to the pure silica. For smaller clusters (number of atoms<250) first peak position shows a remarkable dependence on the structure and size of the cluster. The pair distribution analysis of SAED and HRTEM data indicates a certain degree of ordering with a domain size of ~2nm.

Keywords: electron diffraction, high resolution electron microscopy, rhyolitic glass, nanocrystalline, simulation

1. Introduction

Under ambient conditions, volcanic glass alteration occurs through chemical weathering. The formation of the alteration products mainly depends on interacting water chemistry (Christidis, 2008) and water exposure conditions (e.g. Friedman, Long, 1984, Yokoyama et al. 2008, Hellmann et al. 2012), however the role of the biological activity can also be decisive (Barker, Banfield, 1996, Alt, Mata, 2000, Cuadros et al. 2013a,b). Specific surface and original water content of the volcanic glass affect the dynamics of the alteration as well, thus volcanic glasses like pumice or perlite tends to alter at a higher rate than obsidian does.

At ambient conditions, alteration of silicate minerals mostly occurs via hydration which results hydrated layered silicates, mostly smectites, allophane (Hiradata, Wada, 2005) and other clay minerals (Brownlow, 1996). “Primitive clay” formation on the surface of glass and feldspar has been observed by HRTEM (Tazaki, 1989, 1992). Clay minerals formed during weathering are widely investigated for a long time (e.g. Banfield et al. 1991, de la Fuente et al. 2000, Kawano, Tomita 2001, for overview Velde, Meunier, 2008). At the same time, complete weathering of obsidian into quartz and alunite on a few years timescale, accompanied by supressed clay formation, was also reported recently (Cuadros et al. 2012). This observation indicates that alteration processes can be extremely variable due to a simultaneous control of structural and compositional properties of the source material and environmental factors. Thus, the knowledge of the nanostructure in different stages of the alteration would serve as a good starting point in understanding the alteration processes (e.g. Dalmora et al. 2016, Ramos et al. 2015).

Our present knowledge on the structure of volcanic glasses is mostly based on different spectroscopic and diffraction studies (Wright et al. 1984, Zotov et al. 1989; Deganello et al., 1998, Zotov, 2003, Kis et al. 2006) and conclude a random network of $(Si,Al)O_4$ tetrahedra, similar to silica

glass (for overview see Wright 1994).

In silica glass, theoretical considerations (Gaskell, Wallis 1996), medium range infrared spectra (Görlich 1977, Blaszczak and Görlich 1977), neutron total scattering measurements (Keen, Dove 1999, 2000) and computer simulations (Gladden 1990, Dove et al. 2000) conclude a certain medium range order (MRO) which shows similarities with structural features of the high temperature forms of cristobalite and tridymite over a length scale up to 10 or 20 Å, based on diffraction and specroscopic measurements, respectively. This domain structure theory has recently been visualized by high resolution transmission electron microscopy (HRTEM) in case of two-dimensional amorphous silica (Huang et al. 2012). HRTEM allowed direct imaging of silica rings and determination of ring statistics. It has also been proven that the amorphous silica is composed of different regions ranging from predominantly nanocrystalline to prediminantly amorphous (Huang et al. 2012). Theories and experimental evidences for crystallite-like ordering in network glasses is summarized by Wright (2014).

In this paper we present a detailed nanostructural characterization of a slightly altered rhyolitic volcanic glass, based on TEM methods. Evidences for a few nm scale structural ordering accompanied by increased iron content with respect to the amorphous component have been detected. We give a step-by-step description of the SAED identification of the randomly oriented nanocrystalline component of the volcanic glass and demonstrate that it is dissimilar to smectite clay structure. Experimental data are interpreted by calculating electron scattering curves for silica based nanoclusters of different size, shape and composition.

2. Material and experimental methods

The studied high silica containing rhyolitic volcanic glass is a pumice sample from Tokaj Mts., Hungary (Mineralogical Collection, Eötvös University, Budapest). X-ray powder diffraction (XRPD)

analysis performed by a Philips PW1710 X-ray diffractometer using CuKα radiation at 45 kV and 35 mA and graphite monocromator was carried out to determine the main constituent of the pumice sample. For local structural characterization SAED and HRTEM imaging were performed. Sample preparation was carried out according to the generally established practice (e.g. Sehn et al. 2016). So that, the pumice sample was broken into small parts and examined under binocular microscope. From the debris, fragments showing characteristic glassy fracture were selected for transmission electron microscope (TEM) study. By this procedure we deselected optically distinguishable crystalline parts from the pumice and focused on the glassy component of the rock. Tiny shards of this volcanic glass were carefully ground under ethanol to produce electron transparent pieces and a droplet of the resulting suspension was deposited onto a lacey carbon covered Cu-grid (Ted Pella).

To measure the position of the diffraction rings on SAED patterns with high accuracy, we applied the internal standard method (Figure 1) on a separate TEM specimen prepared as follows. A few nm thick nanocrystalline film was evaporated onto the bottom side of an ultrathin carbon covered Cu-grid, while on the top side a droplet of the sample suspension was deposited. The SAED pattern taken from this specimen contains not only the scattered intensity of the studied material but the diffraction rings of the nanocrystalline gold internal standard as well. This sample preparation method allows us to calibrate the camera length using a single SAED pattern (Figure 1b) and to increase the accuracy of the d-values by approximately an order of magnitude (Sáfrán 2013). We applied gold as an internal standard, because, although being a strong scatterer, it produces stable and well defined diffraction rings without the risk of contamination (e.g. oxidation) which is essential for the exact measurement of the position of diffraction maxima.

a.)

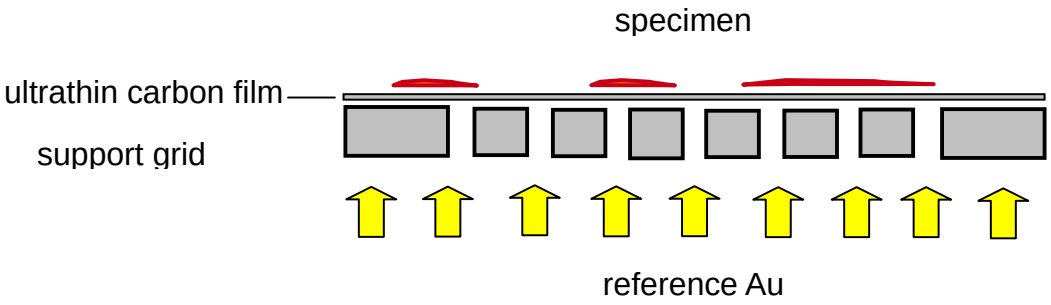

b.)

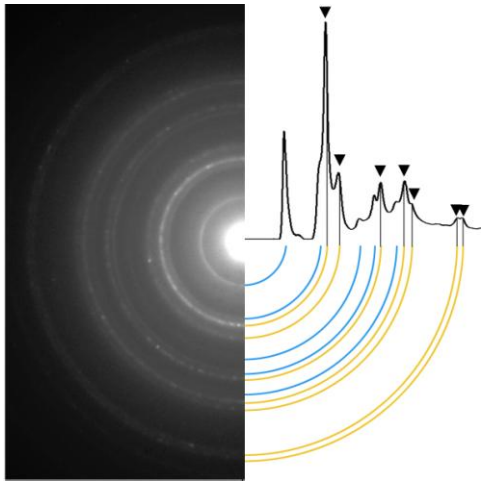

Figure 1: (a) Sample preparation for SAED measurement with internal standard and (b) experimental pattern containing diffraction rings from the studied material (blue rings) and the internal standard (gold rings) used for calibration (marked with ▼).

SAED patterns and chemical analyses were taken on a Philips CM 20 TEM with a LaB_6 cathode, equipped with a Bruker Xflash 5030T energy-dispersive spectrometer (EDS). For chemical analyses, 20-nm spot size and counting times of 100 s were used. The chemical composition was calculated estimating 20 nm sample thickness and an average density of 2.7 g/cm^3. SAED patterns were taken from areas of ca. 250 nm of diameter (if not given else) and each area subjected to diffraction measurement were analyzed chemically subsequently. For the evaluation of the electron

diffraction patterns Process Diffraction (Lábár 2005), software was used. High resolution studies were carried out on a JEOL 3010 UHR with a LaB_6 cathode, equipped with Gatan Imaging Filter Tridiem, and processed with Digital Micrograph (Gatan).

3. Results

X-ray diffraction pattern, acquired from the bulk pumice sample, shows a broad, diffuse amorphous halo (Figure 2) which originates from the main glass component. Additional crystalline peaks are due to minor amount of plagioclase feldspar and a weak indication of some smectitic clay can be observed around 15 Å.

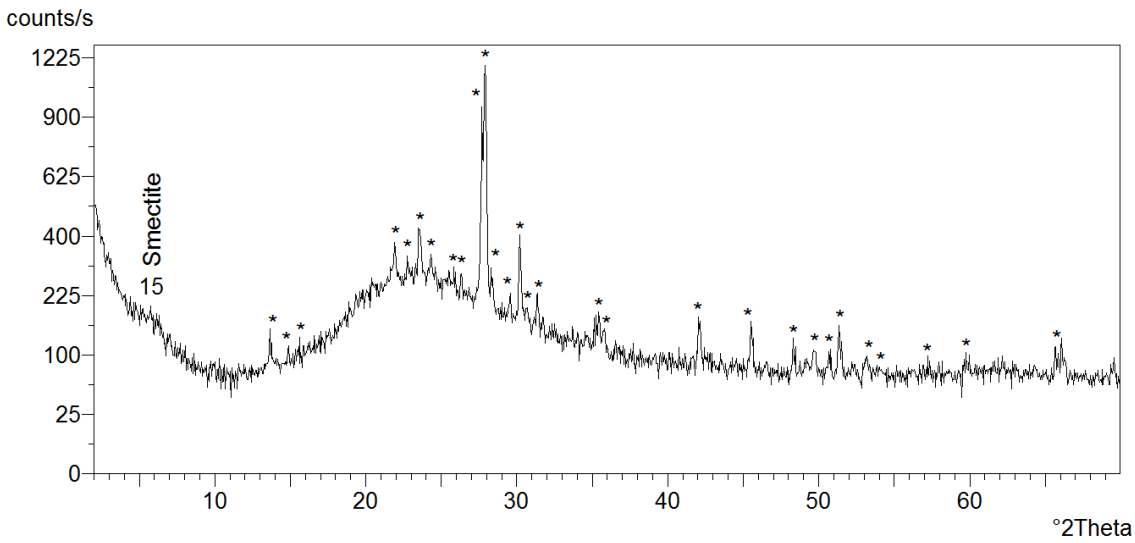

Figure 2: X-ray powder diffraction pattern of Tokaj pumice. Plagioclase reflections are marked by asterisk (*).

The optically selected and crushed glassy fragments were examined by electron diffraction and several

SAED patterns were taken from different particles. Typically, two types of SAED patterns can be distinguished: (1) SAED showing broad diffuse halos at ~4.5 and ~1.5 Å characteristic of amorphous (A) structures, and (2) SAED with several sharp concentric rings, characteristic of nanocystalline (NC) materials (Figure 3). According to EDS analysis (Table 1), NC component of the sample contain iron up to 5 at%, while the iron content of the A component remains below 1 at%.

	O	**Na**	**Mg**	**Al**	**Si**	**K**	**Ca**	**Fe**
nanocrystalline	64.8	0.4	0.8	4.2	23.8	0.5	0.6	5.1
amorphous	67.1	0.9	0.1	5.0	24.6	1.6	0.3	0.4

Table 1: Chemical composition of the amorphous and nanocrystalline components of the glass shards measured by TEM-EDS. The values are given in at% and obtained by averaging 10 independent measurements.

The interplanar spacings in the NC component compared to some relevant structures are given in Table 2.

measured values [Å]	Fe-smectite (hk0)	β-tridymite (hk0)	β-cristobalite
4.45	4.57 (020)	4.35 (100)	4.13 (111)
2.58	2.63 (130)	2.51 (110)	2.53 (220)
1.71	1.69 (310)	1.67 (210)	1.64 (331)
1.51	1.52 (060)	1.44 (300)	1.46 (224)
1.3	1.31 (260)	1.26 (220)	1.26 (440)

Table 2: Interplanar spacings measured on SAED patterns and reference data for nontronite, an iron smectite (Dainyak et al. 2006), β-tridymite (Sato, 1963) and β-cristobalite (Peacor, 1973)

Smectites are characterized by random rotation of subsequent layers (turbostratic structure) which cannot be recognized unambiguously from a diffraction pattern taken from a single projection. Thus, to check if the ring diffraction patterns result from turbostratic smectite, tilt experiments were carried out in the range 0-40°. Turbostratic structure produces ring diffraction pattern only if the electron beam is parallel to the layer normal, in case of smectites to [001]*. By tilting the sample out of this position texture pattern develops: the intensity distribution along the diffraction rings and the shape of the rings themselves gradually changes to produce arcs and at certain angles diffraction spots appear. Natural smectites often show smearing of the diffraction ring when tilted out from hk0 projection (e.g. Zvyagin, 1967). On the other hand, in case of random nanocrystals, the shape of the diffraction rings remains circular independently of the orientation of the sample, however, intensity distribution may change along the ring with tilt angle, depending on the actual orientation of the nanocrystals. By tilt experiments we were able to distinguish some particles showing smeared diffraction rings at 40°, which were identified as smectites, but the majority of the examined particles proved to be randomly oriented nanocrystal (Figure 4).

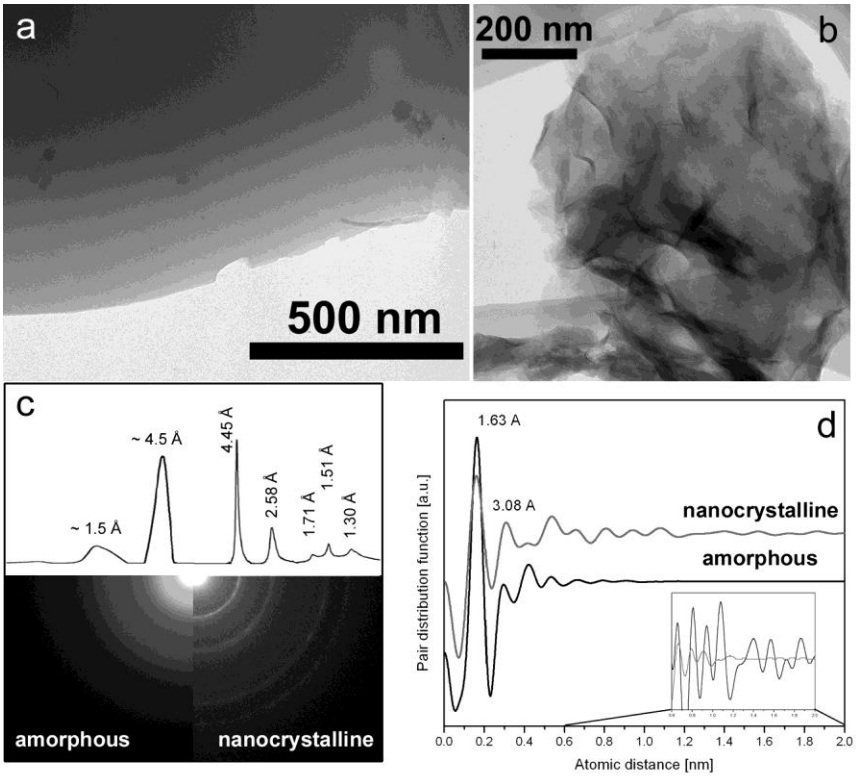

Figure 3: Bright field TEM image of (a) an amorphous area and (b) a nanocrystalline area and (c) the corresponding SAED patterns. Intensity profiles show radial intensity distribution after background subtraction. (d) Pair correlation functions calculated from the SAED patterns.

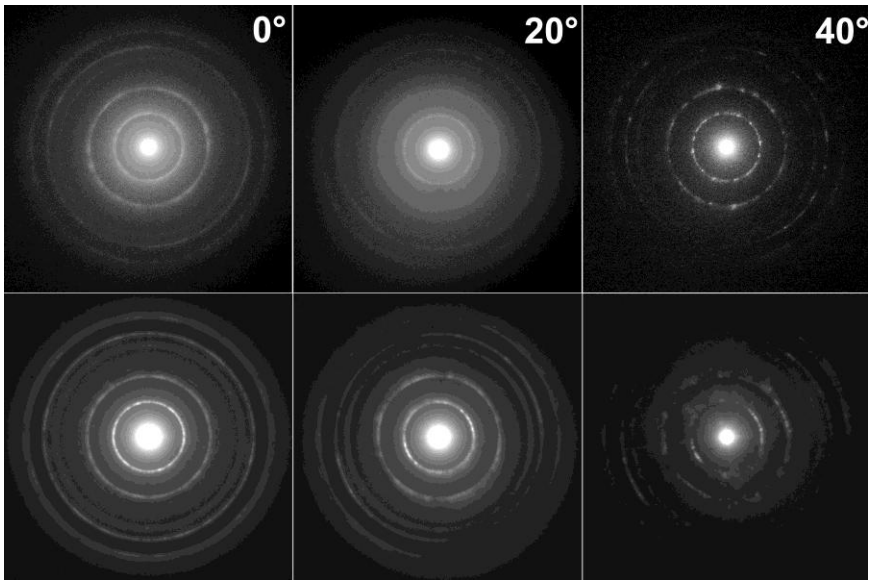

Figure 4: SAED patterns at tilt angles of 0°, 20° and 40° from a particle with randomly oriented nanocrystalline structure (top row) and a smectite particle (bottom row). In case of smectite, smearing of the diffraction rings is evident at 40° tilt.

To quantify the characteristics of the ring diffraction patterns obtained from the NC component, distribution of the diffracted intensity along the innermost diffraction ring was analysed. Intensity was azimuthally integrated along the ring in a 30 px wide band at 0º, 20º and 40º tilt angle and plotted as a function of position (Figure 5). The average intensity value is drawn as straight line for every intensity curve. The measured intensities oscillate uniformly around their average values in the whole range

(from 0º to 360º on Figure 5) with a standard deviation of 9.6 %, 7% and 30% for cases of 0º, 20º and 40º tilt angles, respectively which supports the random orientation of nanocrystals. (Here we note that at 40º tilt a smaller area limiting aperture was used to preserve locality and reduce the effect of the steep change of specimen height. The selected area in this case was 50 nm of diameter, which causes smaller number of coherently diffracting domains, and thus, lower overall values of intensity and higher standard deviation.) Local maximum values (some of them are marked by arrows) are from coherently scattering domains of different size. 60º radial distance between individual maxima is frequent implying hexagonal symmetry inside the nanocrystals. Intensity analysis proved a uniform fluctuation around an average value in case of 0º, 20º and 40º tilt as well, which evidences random nanocrystalline structure.

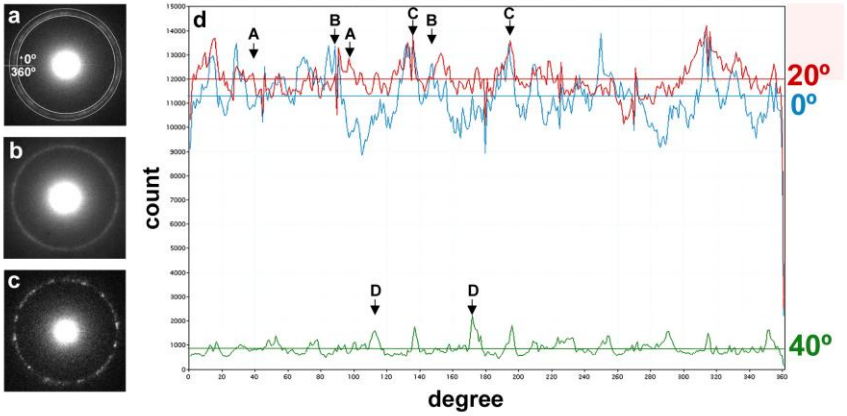

Figure 5: SAED patterns from a nanocrystalline area at (a) 0° (b) 20° and (c) 40° tilt angle. (d) Integrated intensities along the innermost rings at 0° (blue), 20° (red) and 40° (green) tilt angles plotted as a function of position. Straight horizontal lines represent the average values. Capital letters indicate local intensity maxima at 60º radial distance. Note that the SAED pattern at 40° tilt was recorded from an area of ca. 50 nm of diameter.

Figure 5 implies random nanocrystalline structure which is inconsistent with smectite. To obtain the frequency distribution of atomic distances in pair distribution analysis was made on both A and NC SAED patterns (Figure 3d). The most prominent peaks of the pair distribution functions (pdf) are at ~1.6 and ~3.1 Å resulting from the Si-O and Si-Si distance of the structure building blocks of SiO_4 tetrahedra, respectively. The pdf curve from the A component shows no distinct peak beyond 8 Å suggesting no correlation between atoms beyond this distance, however, in the pdf curve of the NC component distinct peaks appear up to 2 nm implying correlated atomic positions up to this distance. The size of the ordered domains can also be estimated using HRTEM (Figure 6) which provides direct imaging of the atomic structure. On the Fourier transform (FT) obtained from the HRTEM image on Figure 6a only the innermost ring appears and careful observation of the image itself allows recognize some white dots organized in hexagonal setting (some of them are marked on Figure 6a) indicating nanocrystalline phase. This HRTEM image represents well the main bulk of the nanocrystalline iron-rich component of the studied volcanic glass and shows a highly disordered nanocrystalline structure with crystalline domain size of less than 5 nm. However on the FT of some HRTEM images (Figure 6b) hexagonal symmetry appears. The Fourier components are arc-shaped which indicates certain degree of rotation between the crystalline domains. The presence of the 2.6 Å periodicity on the FT implies increased order with respect to the structure presented on Figure 6a.

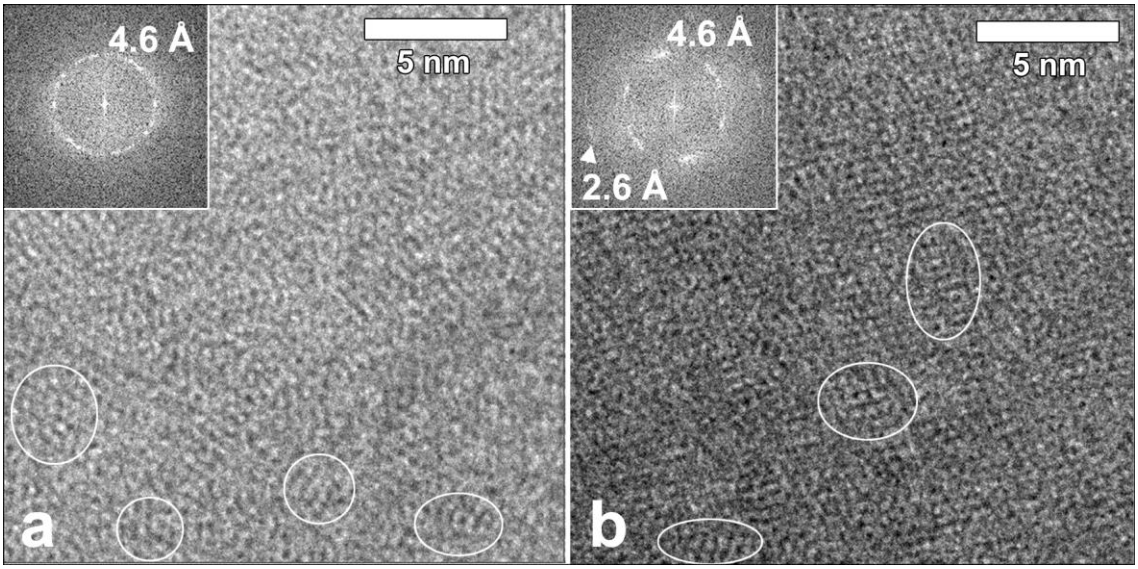

Figure 6: HRTEM images of nanocrystalline areas and the corresponding Fourier transforms. According to FTs, image (a) shows a higher degree of disorder than image (b). Recognizable ordered domains are marked.

4. Discussion

4.1. Scattering by silica clusters

According to XRPD the main constituent of Tokaj pumice is volcanic glass with minor amount of primarily crystallized Ca-feldspar and traces of smectite is detectable as well. The structure of the volcanic glass is amorphous, however TEM revealed the presence of NC component as well. The main points of the TEM-EDS and HRTEM result are that (1) the NC component is characterized by an elevated iron content with respect to the A component (2) the iron-rich NC component has randomly oriented nanostructure and (3) interplanar spacings and radial distance between diffraction maxima imply hexagonal, silica related structure. To get a closer view of the structure of the NC component we calculated the scattered electron intensity for randomly oriented clusters of different size, shape and structure and compared the results with the experimental SAED patterns. Considering the silica dominated chemical composition and the hexagonal symmetry implied by SAED patterns and HRTEM

images, Fd3m (β-) cristobalite was used to generate the atomic coordinates of the input clusters for the calculations. This choice is also supported by our present knowledge about the structure of silica glass. According to X-ray powder diffraction based pair correlation analysis (Gerber, Himmel, 1986), Raman (Sigaev et al. 1999) and middle range infrared (Sitarz et al. 2000) spectroscopy data and neutron total scattering measurements (Keen, Dove 1999, 2000), the structure of amorphous silica over the length scale of up to 10 Å has similarities with that of β-cristobalite. The atomic coordinates of our clusters were not optimized for energy minimum, because the clusters are nor freestanding but embedded in the amorphous matrix.

a) b)

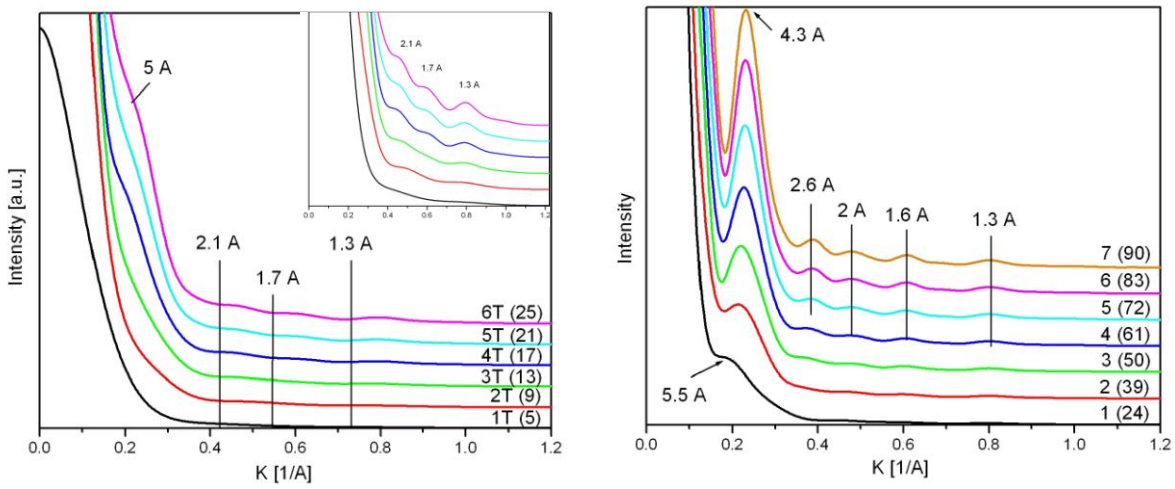

Figure 7: Calculated electron scattering intensity curves for silica clusters of different sizes (a) 1-6 interconnected tetrahedra, (b) 1-7 rings of SiO_4 tetrahedra. The size of the clusters is expressed as number of atoms.

Figure 7 shows the calculated scattered electron intensity distributions for different number of

interconnected SiO_4 tetrahedra. According to the insert of Figure 7a already two interconnected tetrahedra produce some increase in the scattered intensity around ~2 Å and ~1.3 Å. Increasing the cluster size a broad intensity maximum appears around ~1.7 Å as well. These intensity maxima coincide with Bragg peak positions produced by distances between oxygen planes of close packed silica structures and invoke the cristobalite "quasi Bragg" planes discussed by Gaskell and Wallis (1996). At around 5 Å a shoulder appears on the scattered intensity curve calculated for 4 interconnected tetrahedra and becomes more distinct with increasing cluster size. If the tetrahedra are connected to form hexagonal ring the ~5-4.5 Å peak dominates the intensity curve and it shifts towards smaller values for larger cluster size (Figure 7b). The position of this peak is in good agreement with the maximum of the main halo measured on the amorphous SAED patterns and supports that the scattering curve of a single ring reflects nicely the main structural feature of the amorphous regions which is consistent with interpretations of infrared spectroscopy studies (Sitarz et al. 1999, Sitarz 2011). Increasing cluster size is accompanied by the enhancement of the Bragg peaks of the crystalline structure (Figure 6b).

4.2. Scattering by Fe-containing clusters

Cormier and coworkers (e.g. Cormier et al. 1996, 2014) investigated the local environment of transition elements in silicate and borate glasses. Their extended X-ray absorption spectroscopy (EXAFS) and neutron scattering measurements allowed to conclude a considerable cation-cation correlation in corner or edge sharing polyhedra and the development of two-dimensional domains of cations. Based on these results we calculated the scattered electron intensity for iron-containing silica clusters which were generated from β-cristobalite. Iron was inserted into the structure as a two-dimensional hexagonal array of edge sharing FeO_6 polyhedra between two neighbouring silica layers. Edge sharing $Fe(O,OH)_6$ are present in Fe-bearing smectite, nontronite as well (Dainyak et al. 2006),

however, cristobalite- and tridymite-related silica layers sandwiching the octahedral layer appear only in the early structure model of smectites (Edelman, Favejee 1940) which has been applied for the structural interpretation of silica-smectite nanocomposite material (Dódony et al. 2016).

a) b)

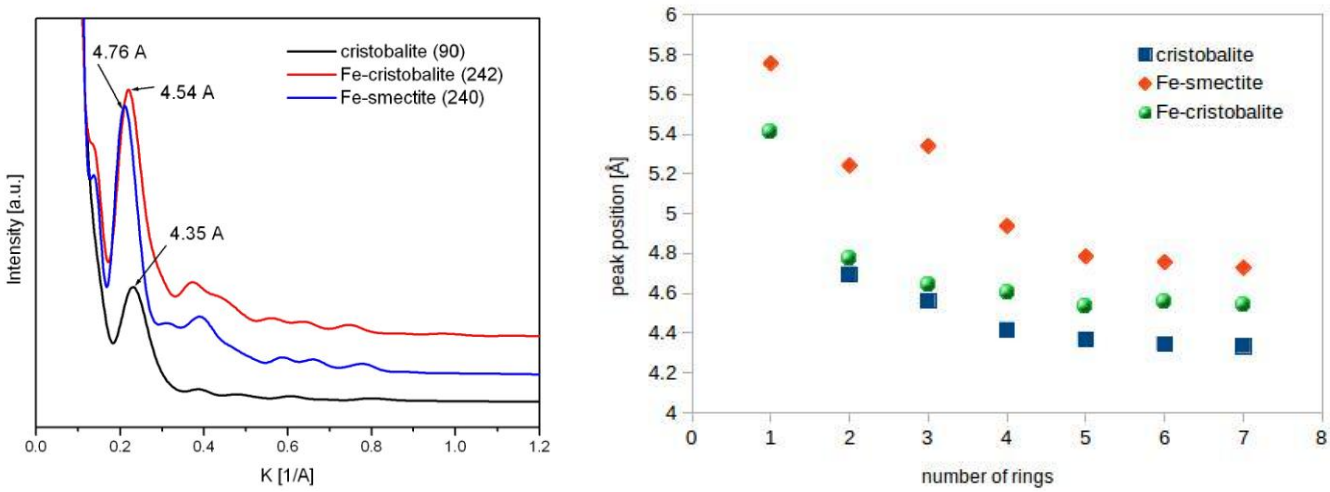

Figure 8: Comparison of calculated electron scattering curves of iron-free and iron-containing clusters. (a) 7 rings of SiO_4 tetrahedra (cristobalite) and 2x7 rings of SiO_4 tetrahedra sandwiching Fe atoms (Fe-cristobalite and Fe-smectite), the arrangement of the rings is shown in the insert, (b) size dependence of the calculated first diffraction peak position for cristobalite, Fe-smectite and Fe-cristobalite.

Figure 8a compares the calculated electron scattering of iron-free and iron containing clusters

with diameter of ca. 1.5-2 nm. Cristobalite cluster contains 7 rings of SiO_4 tetrahedra, while Fe-containing clusters are composed of 2x7 rings of SiO_4 tetrahedra sandwiching an array of Fe atoms. The arrangement of the rings is shown in the insert. In Fe-cristobalite, the silica tetrahedra point alternating up and down with respect to the basal plane (Dódony et al. 2016), which implies continuous network structure. In contrast, in Fe-smectite all of the tetrahedra point towards the array of iron atoms (Dainyak et al. 2006), as it is well known from layer silicate structures.

The most prominent peak appears between 4.3-4.8 Å. Minor peaks are distingusihable at ca. 2.5, 1.5, and 1.3 Å, similarly to the scattering curves of hexagonal rings of SiO_4 tetrahedra (Figure 7b). According to the calculations, the exact position of the first peak depends on the cluster structure and size (Figure 8b). For cristobalite clusters smaller values were obtained (4.35 Å for n=90, 7 rings), while Fe-containing clusters are characterized by larger values (4.76 Å for n=240 and 4.54 Å for n=242 in case of Fe-smectite and Fe-cristobalite, respecticely). With increasing ring number, the position of the first peak decreases approximating the interplanar spacing of the corresponding crystalline polymorphs (Figure 8b, Table 2). This tendency can be explained with the decrease of surface-to-volume ratio, and in connection, lower proportion of incomplete rings, and formation of crystalline planes creating Bragg reflections. The larger values obtained for Fe-containing clusters are due to a less compact structure, which has been formed by the insertion of the iron array in between the silica layers.

Similarities between experimental (Figure 3c) and calculated electron scattering curves is evident which indicates that the inherent structural feature of the random nanocrystalline domains is the formation of six membered rings of SiO_4 tetrahedra. Taking advantage of the accuracy of the experimental peak positions further conclusions can be drawn. According to calculations, iron incorporation into the structure induces peak shift from 4.35 Å of silica up to ~4.8 Å (Figure 8b). Thus, we argue that the measured value of 4.45 Å is therefore an indication of the iron content with a presumable cristobalite-related environment. As the investigated volume of material is nx0.01 μm^3, we also propose that more than one structure type may coexist, and in this case, the measured 4.45 Å peak

position can be explained as an average position, which may vary with the iron content, i.e. cristobalite to Fe-cristobalite (or Fe-smectite) ratio inside the diffracting volume. Indeed, the exact nature of silica layer sandwiching the iron array cannot be stated unambiguously, because the main difference between Fe-smectite and Fe-cristobalite relies in the 00*l* reflections (Dódony et al. 2016).

Regarding the exact position of the first diffraction peak a remarkable dependence on cluster size was observed. Cluster size dependence of diffraction peak positions was reported for planar carbon structures as well, and utilized to derive information on cluster size (Czigany, Hultman 2010). A peak shift up to ±10% was observed in the calculated scattering curves of graphite and graphene nanoclusters with positions approximating the Bragg positions of crystalline graphite with increasing cluster size. In our case, due the calibrated experimental peak position 4.45 Å we estimate that the average size of the random nanocrystalline domains doesn't exceed 250 atoms which means an approximate maximum diameter of 2 nm. In terms of hexagonal rings, this size corresponds to ca. 7 neighbouring rings and agrees with the domain size observed on HRTEM images and the correlation length deduced from pair distribution analysis.

5. Conclusions

The nanostructural characterization of slightly altered silica rich volcanic glass supports the glass domain structure theory of silicate glasses developed based on spectroscopic and diffraction experiments (e.g. Blaszczak, Görlich 1977, Keen, Dove 2000). According to electron diffraction analysis, HRTEM images, and EDS measurements, randomly oriented nanocrystalline and amorphous components were identified. The nanocrystalline component has an approximate domain size around 2 nm and enriched in iron with respect to the amorphous component. The randomly oriented character has been revealed by SAED tilt experiments and the non-smectitic structure was proven. To interpret these SAED patterns, several model clusters were constructed and scattering curves were calculated.

Domains of silica rings has been deduced from electron diffraction measurements. According to our calculations, already a single ring of six interconnected SiO_4 tetrahedra results a separate broad peak at ~5 Å which reflects the main structural feature of amorphous silica. Inserting a two dimensional array of iron between two neighbouring silica layers leads to a shift of the first diffraction peak towards larger values with respect to the pure silica. The shift is larger for Fe-smectite structure (4.76 Å), and it is moderate for Fe-cristobalite (4.54 Å). We propose that Fe incorporation can enhance ordering of the highly polymerized silicate structure while preserving its original cristobalite-like MRO.

Based on the calculations, we conclude that two-dimensional array of iron atoms, sandwiched by silica layers can explain the SAED ring patterns produced by the random nanocrystalline component of the volcanic glass. The deduced domain size is in agreement with experimental SAED and HRTEM data.

Acknowledgements

VKK is grateful to Bolyai János Postdoctotal Fellowship of the Hungarian Academy of Sciences for financial support. This work was supported by Hungarian national Scientific Fund (OTKA Grant number PD 63973).

Captions

Figure 1: (a) Sample preparation for SAED measurement with internal standard and (b) experimental pattern containing diffraction rings from the studied material (blue rings) and the internal standard (gold rings) used for calibration (marked with ▼).

Figure 2: X-ray powder diffraction pattern of Tokaj pumice. Plagioclase reflections are marked by asterisk (*).

Figure 3: Bright field TEM image of (a) an amorphous area and (b) a nanocrystalline area and (c) the corresponding SAED patterns. Intensity profiles show radial intensity distribution after background subtraction. (d) Pair correlation functions calculated from the SAED patterns.

Figure 4: Bright field TEM image of (a) an amorphous area and (b) a nanocrystalline area and (c) the corresponding SAED patterns. Intensity profiles show radial intensity distribution after background subtraction. (d) Pair correlation functions calculated from the SAED patterns.

Figure 5: SAED patterns from a nanocrystalline area at (a) 0° (b) 20° and (c) 40° tilt angle. (d) Integrated intensities along the innermost rings at 0° (blue), 20° (red) and 40° (green) tilt angles plotted in function of position. Straight horizontal lines represent the average values. Capital letters indicate local intensity maxima at 60º radial distance. Note that the SAED pattern at 40° tilt was recorded from an area of ca. 50 nm of diameter.

Figure 6: HRTEM images of nanocrystalline areas and the corresponding Fourier transforms. According to FTs, image (a) shows a higher degree of disorder than image (b). Recognizable ordered domains are marked.

Figure 7: Calculated electron scattering intensity curves for silica clusters of different sizes (a) 1-6 interconnected tetrahedra, (b) 1-7 rings of SiO_4 tetrahedra. The size of the clusters is expressed as number of atoms.

Figure 8: Comparison of calculated electron scattering curves of iron-free and iron-containing clusters. (a) 7 rings of SiO_4 tetrahedra (cristobalite) and 2x7 rings of SiO_4 tetrahedra sandwiching Fe atoms (Fe-cristobalite and Fe-smectite), the arrangement of the rings is shown in the insert, (b) size dependence of the calculated first diffraction peak position for cristobalite, Fe-smectite and Fe-cristobalite.

Table 1: Chemical composition of the amorphous and nanocrystalline components of the glass shards measured by TEM-EDS. The values are given ni at% and obtained by averaging 10 independent measurements.

Table 2: Interplanar spacings measured on SAED patterns and reference data for nontronite, an iron smectite (Dainyak et al. 2006), β-tridymite (Sato, 1963) and β-cristobalite (Peacor, 1973)

References

Alt, J.C. and Mata, P. (2000) On the role of microbes in the alteration of submarine basaltic glass: a TEM study. *Earth and Planetary Science Letters*, **181**, 301–313

Banfield, J.F., Jones, B.F., Veblen, D.R. (1991): An AEM-TEM study of weathering and diagenesis, Abert Lake, Oregon: I. Weathering reactions in the volcanics. *Geochim. Cosmochim. Acta*, **55**, 2781-2793.

Barker, W.W. and Banfiled, J.F. (1996): Biologically versus inorganically mediated weathering reactions: relationships between minerals and extracellular microbial polymers in lithobiontic communities. *Chemical Geology*, **132**, 55–69.

Brownlow, A.H. (1996) Geochemistry, 580 p. Prentice Hall, New Jersey.

Christidis, G. (2008) Do bentonites have contradictory characteristics? An attempt to answer unanswered questions. *Clay Minerals*, **43**, 515–529.

Cormier, L., Cochain, B., Dugu, A., Dargaud, O. (2014): Transition Elements and Nucleation in Glasses Using X-ray Absorption Spectroscopy. *Int. J. of Applied Glass Science*, **5 [2]**, 126–135. DOI:10.1111/ijag.12073

Cormier, L., Creux, S., Galoisy, L., Calas, G., Gaskell , P.H. (1996): Medium range order around cations in silicate glasses. *Chemical Geology*, **128,** 77-91.

Cuadros, J., Afsin, B., Jadubansa, P., Ardakani, M. Ascaso, C., Wierzchos, J. (2013a): Pathways of volcanic glass alteration in laboratory experiments through inorganic and microbially-mediated processes. *Clay Minerals*, **48**, 423–445.

Cuadros, J., Afsin, B., Jadubansa, P., Ardakani, M. Ascaso, C., Wierzchos, J. (2013b):Microbial and inorganic control on the composition of clay from volcanic glass alteration experiments. *American Mineralogist*, **98**, 319–334.

Cuadros, J., Afsin, B., Michalski, J.R., Ardakani, M. (2012): Fast, microscale-controlled weathering of

rhyolitic obsidian to quartz and alunite. *Earth and Planetary Science Letters,* **353–354,** 156–162.

Czigany Zs., Hultman L. (2010): Interpretation of electron diffraction patterns from amorphous and fullerene-like carbon allotropes. *Ultramicroscopy,* **110,** 815–819.

de la Fuente, S., Cuadros, J., Fiore, s., Linares, J. (2000): Electron microscopy study of volcanic tuff alteration to illite-smectite under hydrothermal conditions. *Clays and Clay Minerals*, 48, 339-350, 2000.

Dainyak, L.G., Zviagina B.B., Rusakov V.S. Drits V.A. (2006): Interpretation of the nontronite-dehydroxylate Mössbauer spectrum using EFG calculations. *Eur. J. Mineral.*, **18**, 753-764.

Dalmora, A.C., Ramos, C.G., Querol, X., Kautzmann, R.M., Oliveira, M.L.S, Taffarel, S.R., Moreno, T., Silva, L.F.O. (2016): Nanoparticulate mineral matter from basalt dust wastes. *Chemosphere,* **144**. 2013-2017.

Dódony, I., Németh, T. & Kovács Kis, V. (2016): Report on the natural occurrence of a silica-clay nanocomposite *Resolution and Discovery,* **1,** DOI: 10.1556/2051.2016.00018

Deganello, G., Liotta, L., Longo, A., Martorana, A., Yanev, Y., Zotov, N. (1998): Structure of natural water-containing glasses from Lipari (Italy) and Eastern Rhodopes (Bulgaria): SAXS, WAXS, and IR studies. *J. Non-Cryst. Solids*, **232–234**, 547–553.

Dove, M.T., Hammonds, K.D., Harris, M.J., Heine, V., Keen, D.A., Pryde, A.K.A., Trachenko, K. Warren, M.C. (2000): Amorphous silica from the Rigid Unit Mode approach. *Mineral. Mag.*, **64**, 377-88.

Edelman, C.H. & Favejee, J.Ch.L. (1940): On the crystal structure of montmorillonite and halloysite. *Z. Kristallogr*., **102**, 417-431.

Friedman, I. and Long, W. (1984): Volcanic glasses, their origins and alteration processes. *J. Non-Cryst. Sol*., **67,** 127-133.

Gaskell, P.H., Wallis, D.J. (1996): Medium-Range Order in Silica, the Canonical Network Glass. *Phys. Rev. Letters,* **76. 1**., 66-69.

Gerber, T. & Himmel, B. (1986): The structure of silica glass. *J. Non-Cryst. Solids,* **83,** 324-334.

Gladden, L.F. (1990): Medium-rande order in v-SiO_2. *J. Non-Cryst. Solids,* **119,** 318-330.

Görlich, E. (1977): Structure and phase transformations in glass. *Rev. int. Htes Temp. Refract.,* **14,** 201-206.

Görlich, E., Blaszczak, K. (1977): Polymorphic transition in silica glass. *Nature,* **6,** 265.

Hellmann, R., Wirth, R., Daval, D., Barnes, J-P., Penisson, J-M, Tisserand, D., Epicier, T., Florin, B., Hervig, R.L. (2012): Unifying natural and laboratory chemical weathering with interfacial dissolution–reprecipitation: A study based on the nanometer-scale chemistry of fluid–silicate interfaces. *Chemical Geology,* **294–295,** 203–216.

Hiradata, S. and Wada, S (2005): Weathering process of volcanic glass to allophane determined by ^{27}Al and ^{29}Si solid-state NMR. *Clay and Clay Min*., **53,** 401-408.

Huang, P.Y., Kurasch, S., Srivastava, A., Skakalova, V., Kotakoski, J., Krasheninnikov, A.V., Hovden, R., Mao, Q., Meyer, J.C., Smet, J., Muller, D.A., Kaiser, U. (2012): Direct Imaging of a Two-Dimensional Silica Glass on Graphene. *Nano Lett*., **12**, 1081−1086

Kawano, M. and Tomita, K. (2001): TEM-EDX study of weathered layers on the surface of volcanic glass, bytownite, and hypersthene in volcanic ash from Sakurajima volcano, Japan. *American Mineralogist*, **86,** 284-292.

Keen, D.A. and Dove, M.T. (1999): Comparing the local structures of amorphous and crystalline polymorphs of silica. *J. Phys.: Cond. Matter*, **11**, 9263-73.

Keen, D.A. and Dove, M.T. (2000): Total scattering studies of silica polymorphs: similarities in glass and disordered crystalline local structure. *Miner. Mag*., **63(3),** 447-457.

Kis, V.K., Dódony,, I., Lábár, J.L. (2006): Amorphous and partly ordered structures in SiO 2 rich volcanic glasses. An ED study. *Eur. J. Mineral*., **18**, 745–752

Lábár, J.L. (2005): Consistent indexing of a (set of) SAED pattern(s) with the ProcessDiffraction program, *Ultramicroscopy,* **103,** 237-249.

Peacor, D. R. (1973): High-temperature single-crystal study of the cristobalite inversion. *Z. Kristallogr.*, **138**, 274-298.

Ramos, C.G., Querol, X., Oliveira, M.L.S., Pires, K., Kautzmann, R.M., Oliveira, L.F.S (2015): A preliminary evolution of volcanic rock powder for application in agriculture as soil a remineralizer. *Science of the Total Environment*, **512-513**, 371-380.

Sáfrán, G. (2013): Calibration of HRTEM for lattice parameter measurements in nanocrystals Proc. Microscopy Congress Regensburg, Germany. (ed. Reinhard Rachel) 2013.08.25-0213.08.30. 89-90.

Sato M. (1963): X-ray study of tridymite (1). On tridymite M and tridymite S. *Mineral. J. (Japan)*, **4**, 115-130.

Sehn, J.L., De Leão, F.B., Da Boit, K., Oliveira, M. L.S., Hidalgo, G. E., Sampaio, C.H., Silva, L.F.O. (2016): Nanomineralogy in the real world: A perspective on nanoparticles in the environmental impacts of coal fire. *Chemosphere,* **147**. 439-443.

Sigaev, V.N., Smelyanskaya, E.N., Plotnichenko, V.G., Koltashev, V.V., Volkov, A.A. & Pernice, P. (1999): Low frequency band at 50 cm^{-1} in the Raman spectrum of cristobalite: identification of similar structural motifs in glasses and crystals of similar composition. *J. Non-Cryst. Solids,* **248,** 141-146.

Sitarz, M., Mozgawa, W., Handke, M. (1999): Rings in the structure of silicate glasses. Journal of *Molecular Structure,* **511–512,** 281–285.

Sitarz, M., Handke, M., Mozgawa, W. (2000): Identification of silicooxygen rings in SiO 2 based on IR spectra. *Spectrochimica Acta Part A,* **56,** 1819 – 1823.

Sitarz, M. (2011): The structure of simple silicate glasses in the light of Middle Infrared spectroscopy studies. *J. Non-Cryst. Solids,* **357,** 1603–1608.

Takazi, K., Fyfe, W.S., van der Gaast, S.J. (1989): Growth of clay minerals in natural and synthetic glasses. *Clays and Clay Min*., **37,** 348-354.

Tazaki, K., Tiba, T., Aratani, M., Miyachi, M. (1992): Structural water in volcanic glass. *Clays and Clay Min*., **40,** 122-127.

Velde, B.B., Meunier, A. (2008): The Origin of Clay Minerals in Soils and Weathered Rocks. Springer, 406 p. ISBN: 978-3-540-75633-0

Wright, A.C., Erwin Desa, J.A., Weeks, R.A., Sinclair, R.N., Bailey, D.K. (1984): Neutron diffraction studies of natural glasses. *J. Non-Cryst. Solids*, **67**, 35–44.

Wright, A.C. (1994): Neutron scattering from vitreous silica. V. The structure of vitreous silica: What have we learned from 60 years of diffraction strudies? *J. Non-Cryst. Solids,* **179,** 84-115.

Wright, A.C. (2014): Crystalline-like ordering in melt-quenched network glasses? *J. of Non-Cryst. Solids,* **401,** 4–26.

Yokoyama, T., Okumura, S., Nakashima, S. (2008): Hydration of rhyolitic glass during weathering as characterized by IR microspectroscopy. *Geochimica et Cosmochimica Acta,* **72,** 117–125.

Zotov, N. (2003): Structure of natural volcanic glasses: diffraction versus spectroscopic perspective. *J. Non-Cryst. Solids*, **323**, 1–6.

Zotov, N., Dimitrov, V., Yanev, Y. (1989): X-ray radial distribution function analysis of acid volcanic glasses from the Eastern Rhodopes, Bulgaria. *Phys. Chem. Minerals*, **16**, 774–782.

Zvyagin, B.B. (1967): Electron diffraction analysis of clay mineral structures. Plenum Press, New York. ISBN-13: 978-1-4615-8614-2

Nanostructural investigation of slightly altered rhyolitic volcanic glass

Viktoria Kovács Kis, Zsolt Czigány, Tibor Németh

Highlights:

- Nanocrystalline and amorphous components are distinguished within rhyolitic volcanic glass using electron diffraction and high resolution electron microscopy.
- Nanocrystalline component is enriched in iron with respect to the amorphous component.
- Electron diffraction tilt experiments prove that nanocrystalline component is randomly oriented with cristobalie-related structure.
- Calculated electron scattering curves indicate that the position of the first diffraction peak has a remarkable dependence on cluster size and iron content.